

Synthesis and Photoluminescence of Assembly-Controlled ZnO Architectures by Aqueous Chemical Growth

Feng Xu, Yinong Lu, Yan Xie, and Yunfei Liu

J. Phys. Chem. C, **2009**, 113 (3), 1052-1059 • DOI: 10.1021/jp808456r • Publication Date (Web): 29 December 2008

Downloaded from <http://pubs.acs.org> on February 12, 2009

More About This Article

Additional resources and features associated with this article are available within the HTML version:

- Supporting Information
- Access to high resolution figures
- Links to articles and content related to this article
- Copyright permission to reproduce figures and/or text from this article

[View the Full Text HTML](#)



ACS Publications
High quality. High impact.

Synthesis and Photoluminescence of Assembly-Controlled ZnO Architectures by Aqueous Chemical Growth

Feng Xu, Yinong Lu,* Yan Xie, and Yunfei Liu

State Key Laboratory of Materials-Oriented Chemical Engineering, College of Materials Science and Engineering, Nanjing University of Technology, Nanjing 210009, China

Received: September 23, 2008; Revised Manuscript Received: October 31, 2008

ZnO rod arrays were directly grown on In₂O₃/Sn (ITO)-coated glass substrates without needing a preprepared ZnO seed layer by aqueous chemical growth (ACG) using an equimolar aqueous solution of Zn(NO₃)₂·6H₂O and C₆H₁₂N₄. By further varying the substrates such as glass, Pt/glass, and Au/glass, other assembly patterns of ZnO architectures (rodlike, flowerlike, urchinlike, and stelliform crystals) were also obtained. The possible growth mechanisms for different assembly patterns dependent on the substrate were proposed. It was revealed that both the inherent highly anisotropic structure of ZnO and the surface energy minimization of different substrates play crucial roles in determining final morphologies of ZnO architectures. In addition, the photoluminescence (PL) properties of ZnO architectures on various substrates were investigated at room temperature.

1. Introduction

Zinc oxide (ZnO), an important semiconductor material with a direct band gap ($E_g = 3.37$ eV), has triggered great interest in the past decade due to its possible use as optoelectronic devices in the short wavelength and ultraviolet (UV) portion of the electromagnetic spectrum.¹ Compared with other wide band gap materials (e.g., ZnSe, GaN, SnO₂, and ZnS), ZnO has a higher exciton binding energy ($E_{ex} = 60$ meV) at room temperature, which is advantageous for exciton-related device applications.² Until now, a room temperature UV lasing effect with intensive optical pumping has been obtained.³ Moreover, ZnO has been extensively investigated because of its great potential use for piezoelectric transducers,⁴ optical waveguides,⁵ surface acoustic wave filters,⁶ chemical and gas sensors,⁷ light-emitting diodes,⁸ dye-sensitized solar cells (DSSCs),⁹ and so forth.

The control over assembly and morphology of nanometer- and micrometer-sized ZnO as thin film on various substrates represents a great challenge to realize the development of novel functional devices. This is because optical and electronic properties of ZnO film, which finally determine practical applications, can be modulated by varying its assembly and morphology.^{10,11} Over the past years, special attention has been devoted to nanometer- and micrometer-sized ZnO of one-dimensional (1D) structures, such as wires or rods,^{12–14} fibers,^{15,16} tubes,¹⁷ coaxial cables,¹⁸ and belts or ribbons,¹⁹ and of complex architectures based on 1D structures, such as branches,²⁰ urchins,²¹ and networks.²² These morphologies may provide opportunities to exploit novel properties due to unique 1D structures and explore possible new phenomena arising from hierarchical structures. A large number of techniques have been exploited to fabricate various crystal morphologies of ZnO films. Among these, thermal evaporation,^{23–26} chemical vapor deposition (CVD),²⁷ molecular beam epitaxy (MBE),²⁸ and sputtering²⁹ commonly require high temperature or vacuum and costly equipments.

To reduce the cost of synthesis, solution methods have triggered increasing interest and have been employed to grow nano/microstructured ZnO. Among all the solution methods such as hydrothermal process^{30,31} and aqueous chemical growth (ACG),^{32,33} ACG has been demonstrated to be a simple approach to develop ZnO films without any intricate equipment. ACG has attracted particular interests for its potential for large-scale deposition and flexible processes on various substrates. However, the systematical control of crystal evolution still remains a great challenge. In addition, the mechanism for the formation of different morphologies of crystal is far from being fully understood. In this work, we investigate the possibility of synthesis of assembly controlled ZnO architectures by ACG on different substrates, including glass, In₂O₃/Sn (ITO)-coated glass, and Au- or Pt-sputtering glass. Other external factors, such as reaction time, solution temperature, and precursor concentration, have also been studied for obtaining different morphologies of ZnO crystals. Toward this goal, preliminary results are presented related to the growth and assembly of ZnO architectures. Detailed growth mechanisms for ZnO architectures on various substrates were discussed tentatively. In addition, room temperature photoluminescence (PL) properties of as-synthesized ZnO samples were investigated too.

2. Experimental Section

All chemicals purchased from Shanghai Chemical Reagents Co. Ltd. were of analytical reagent grade and used as received without further purification. Microscope glass slides and ITO glass were cut into 20 × 20 mm² slices and then cleaned in deionized water, ethanol, and acetone. Au/glass or Pt/glass substrates were prepared by Au- or Pt-sputtering on pretreated glass slides using an auto fine coater (JFC-1600, JEOL Ltd., Japan). In a typical experiment, an equimolar (0.005–0.05 M) aqueous solution of zinc nitrate (Zn(NO₃)₂) and hexamethylenetetramine (C₆H₁₂N₄, HMT) was prepared as the precursor solution. Pretreated substrates for the direct growth of ZnO were immersed in the bottle filled with the above precursor solution. Notably, the ITO, Au/glass, and Pt/glass substrates were placed face down in the solution, to avoid additional deposition of

* To whom correspondence should be addressed. Phone: +86 25 83587248. Fax: +86 25 83587251. E-mail: ynlu@njut.edu.cn.

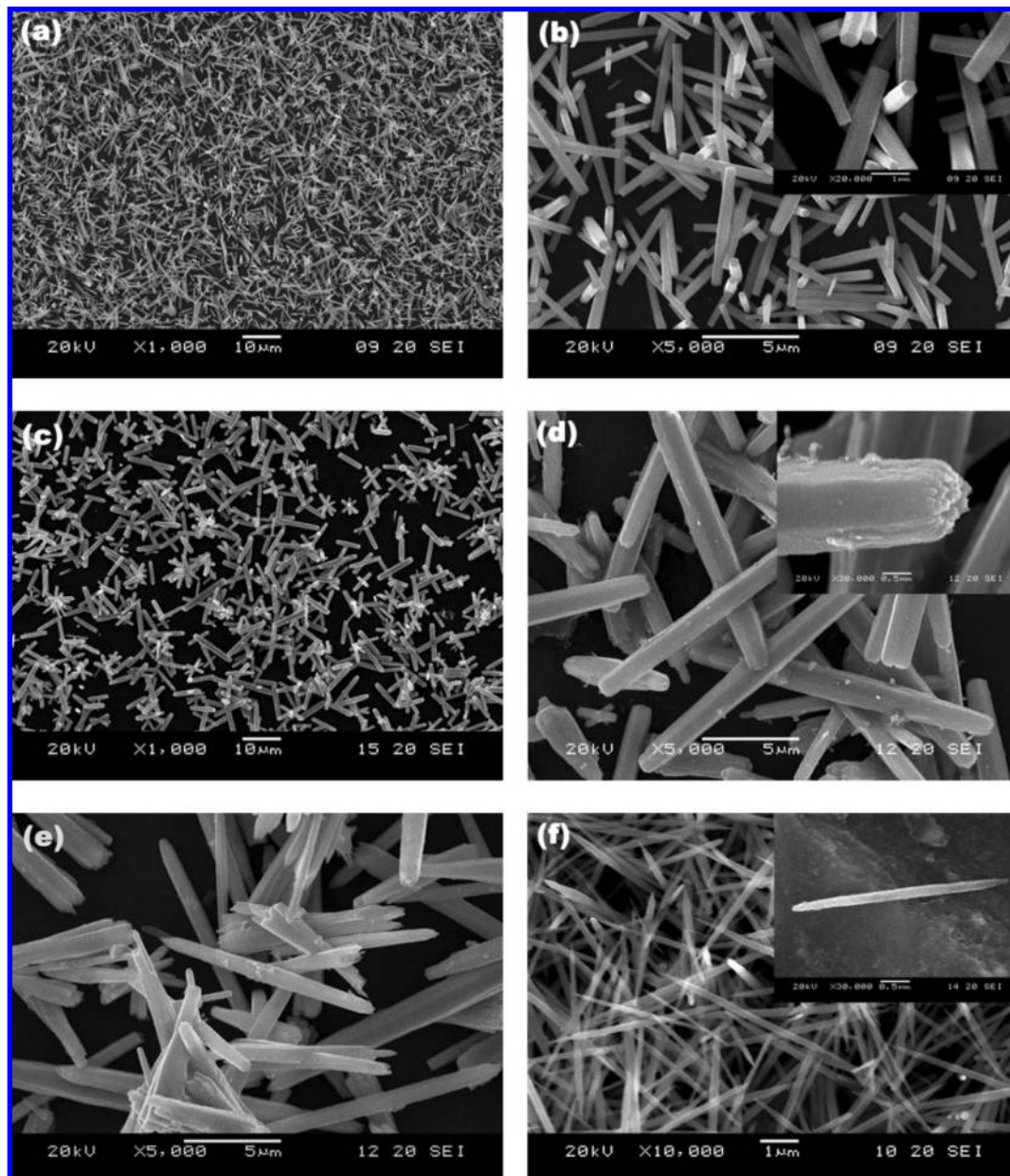


Figure 1. Plan view SEIs of ZnO architectures grown on glass substrates under different growth conditions: (a, b) 0.005 M, 70 °C, 3 h; (c, d) 0.05 M, 90 °C, 6 h; (e) 0.05 M, 90 °C, 18 h; (f) 0.05 M, 90 °C, 27 h. The up-right insets in (a)–(c) show the enlarged view of the representative individual crystal.

particles.³⁴ Then, the bottle was sealed and heated at a constant temperature of 70–90 °C for 3–27 h. After each growth period, the samples were thoroughly washed with deionized water in order to eliminate residual salts and dried in the oven at 60 °C for 2 h.

The secondary electron images (SEIs) from a scanning electron microscope (SEM, JSM-5900, JEOL Ltd., Japan) were employed for the observation of the surface morphology of the deposited samples. Chemical compositions of the as-prepared samples were obtained using an energy-dispersive spectrometer (EDS, Noran Vantage DSI, Thermo Noran, Middleton, WI). Their crystallographic characterization was investigated by an X-ray diffractometer (XRD, ARL XTRA, Thermo Electron Co., Waltham, MA) with Cu $K\alpha_B$ radiation. Transmission electron microscopic (TEM) images were performed with a high-resolution transmission electron microscope (HRTEM, JEM-2010, JEOL Ltd., Japan). The room-temperature photoluminescence (PL) spectra were measured with a spectrophotometer

(Jobin Yvon Fluorolog3-221) using a Xe lamp (450 W) as the excitation source at an excitation wavelength of 325 nm.

3. Results and Discussion

The aim of these experiments was to study the possibility of synthesis of assembly controlled ZnO architectures on different substrates by varying external solution factors. Therefore, the effects of different substrates on assembly of ZnO architectures should be investigated in detail. Figure 1 shows the typical plan view SEIs of ZnO architectures grown on glass substrates under different growth conditions. When the precursor concentration was 0.005 M and the bath temperature was 70 °C, ZnO crystals having a long hexagonal rodlike shape were obtained after a 3 h growth duration, as displayed in Figure 1a and b. These crystals were sharply angulated and showed well-defined hexagonal facets of 300 nm in diameter (inset of Figure 1b) and 6 μm in length. The aspect ratio of the rodlike ZnO crystals

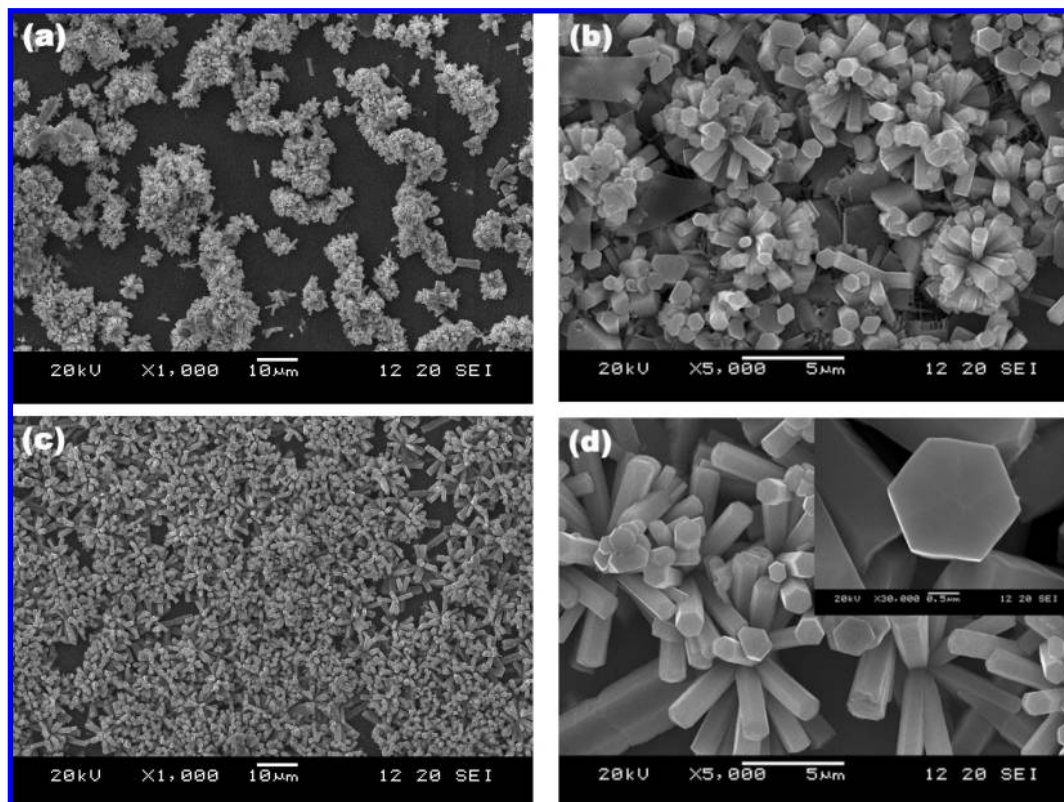


Figure 2. Plan view SEIs of ZnO architectures grown on Pt/glass substrates under different growth conditions: (a, b) 0.005 M, 70 °C, 3 h; (c, d) 0.05 M, 90 °C, 6 h. The up-right inset in (d) shows the enlarged view of the typical hexagonal end plane.

was estimated to be about 20 (6000 nm/300 nm) from the SEIs. In addition, we can also see from Figure 1a and b that these ZnO nanorods are in high density and randomly orientated on glass substrates with little evidence for perpendicular growth. When the precursor concentration and the bath temperature were respectively increased to 0.05 M and 90 °C, ZnO samples still show a long rodlike shape (Figure 1c and d) after a 6 h growth duration, with the only difference being the size of the ZnO rods and the coverage of the substrate area. These ZnO rods are about 1.5 μm in diameter and 10–15 μm in length, respectively. It is noticeable that the end faces of these microrods seem to be “dissolved” and the hexagonal contour is rough and invisible (inset of Figure 1d). With the growth duration increasing to 18 h, the evidence of “dissolution” of ZnO rods is more evident, and double-tip rods were yielded, as shown in Figure 1e. For a longer growth duration of 27 h, large-scale double-tip ZnO needles were synthesized on the glass substrate, as shown in Figure 1f. In the previous report,³⁵ single-tip needle-shaped ZnO nanowires have been fabricated on silicon substrate via the complicated thermal evaporation of metallic zinc powder at a high temperature of 600 °C. Compared with those samples having only a needle tip, our nanoneedles exhibit novel double-tip morphology, which has not been reported for ZnO synthesis by ACG and other techniques up to now. The typical diameters of the obtained products at their middles and tips range between 100 and 150 nm and between 20 and 30 nm, respectively, and the typical lengths are in the range 4–6 μm (inset of Figure 1f).

Figure 2 shows the typical plan view SEIs of ZnO architectures grown on Pt-sputtering glass substrates. Under the condition of low temperature (70 °C) and low precursor concentration (0.005 M), flowerlike ZnO bunches began to come into being, as displayed in Figure 2a and b. Each bunch is composed of closely packed submicrometer-sized rods with diameters of

400–600 nm and lengths of 2–3 μm and forms radiating architectures. Interestingly, these ZnO bunches seemed to root in some special sites on Pt/glass substrates and no longer distributed randomly in the form of single rod, which indicates that ZnO crystallites have been able to nucleate and grow on Pt/glass substrates. When the precursor concentration and the bath temperature were respectively increased to 0.05 M and 90 °C, similar flowerlike ZnO bunches (Figure 2c and d) still existed after a 6 h growth duration. In fact, the ZnO architectures much resemble a beautiful flower in morphology. In any case, all grown architectures consisted of hexagonal prismatic rods (inset of Figure 2d), indicating the nature of the hexagonal wurtzite ZnO crystal structure.

The SEIs of ZnO architectures synthesized on Au-sputtering glass substrate are illustrated in Figure 3. It can be seen from Figure 3a and b that short growth duration (3 h) resulted in the formation of naillike ZnO crystals with a single tip. These nails are approximately 300 nm in end diameter and 2 μm in length. Surprisingly, large numbers of ZnO nanonails erected grew on the Au/glass substrate with the tip downward. With increasing precursor concentration and bath temperature to 0.05 M and 90 °C, respectively, stelliform ZnO crystals were obtained (Figure 3c and d). These stelliform crystals are composed of one long rod standing erectly on the substrate (marked with some arrows in Figure 3c and d) and several rods growing radially at the bottom of the erectly grown rod. All these imply that Au crystallites could act as nucleation sites for ZnO growth. To validate this, a glass slice sputtered with Au for a longer time was used as the substrate for the synthesis of ZnO crystals. The SEIs of the obtained sample (Figure 3e and f) reveal that a bulk quantity of urchinlike ZnO architectures densely exists. More Au crystallites on the glass substrate should account for the densely distributed morphology due to more nucleation sites for ZnO growth.

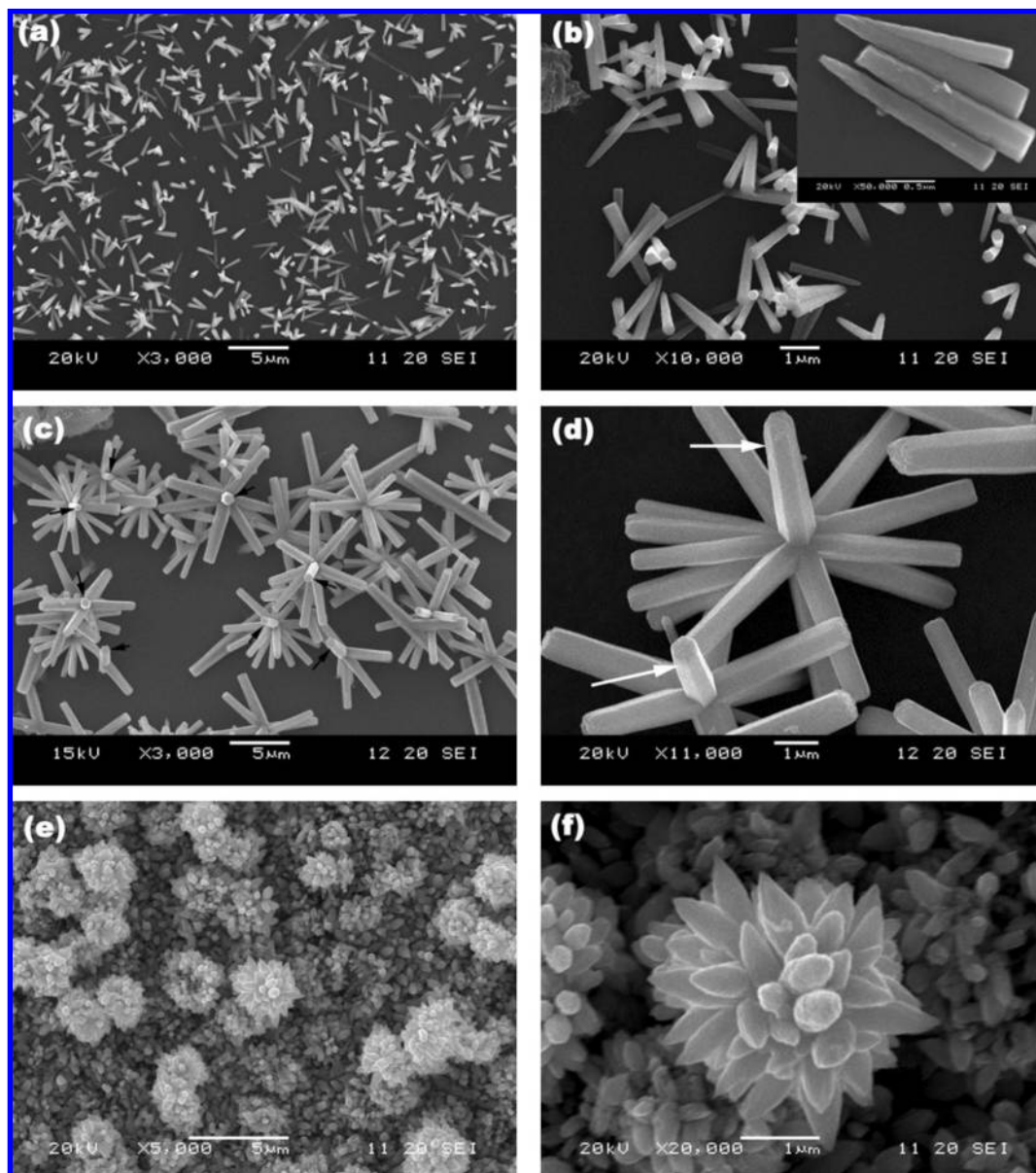


Figure 3. Plan view SEIs of ZnO architectures grown on Au/glass substrates under different growth conditions: (a, b) 0.005 M, 70 °C, 3 h; (c, d) 0.05 M, 90 °C, 6 h; (e, f) 0.05 M, 90 °C, 3 h. The up-right inset in (b) show the enlarged view of some separate naillike crystals.

Obviously, the status of the substrates plays a significant effect on the morphology and assembly of ZnO architectures. Subsequently, a series of experiments on ITO substrates were performed, and the SEIs of the as-prepared samples are selectively shown in Figure 4. Compared with the above-mentioned samples, the morphologies of the samples on ITO substrates were found to be dramatically different. The SEIs of the samples synthesized at a low precursor concentration of 0.005 M and low bath temperature of 70 °C show a large area of vertically aligned ZnO rod arrays (ZRAs) on ITO substrates (Figure 4a and b), and the coverage is dependent on the growth time. Figure 4c–f witness different growth stages of ZnO samples at a high precursor concentration of 0.05 M and a high bath temperature of 90 °C. Figure 4c reveals the presence of ZnO crystallites nucleated directly on the ITO substrate at the initial nucleation period. Figure 4d and e shows the subsequent growth period of ZnO rods on the basis of ZnO nuclei. Ultimately, large numbers of ZRAs over the entire ITO substrate were successfully obtained, as shown in Figure 4f. These ZRAs are highly oriented along their *c*-axes perpendicular to the

substrate with a diameter of 600–800 nm and a length of about 1.5 μm (inset of Figure 4f). Further structural characterizations of the ZnO rods were performed by TEM and HRTEM. To prepare TEM samples, the ZnO rods were scraped from the ITO glass substrate onto an amorphous holey carbon film coated copper grid. Figure 4g shows the low-resolution TEM image of an individual single-crystalline ZnO nanorod with diameter of 500 nm. The corresponding SAED pattern of the ZnO nanorod (inserted at the up-left corner of Figure 4g) can be indexed to the wurtzite structure of hexagonal ZnO and indicates its single-crystalline nature and its growth direction along [0001]. The typical HRTEM image, taken from the area marked with the black frame in Figure 4g, is illustrated in Figure 4h. The crystal lattice fringes are clearly detected, and the average distance between the adjacent lattice planes is 0.26 nm that also corresponds well to the interplanar distance of the {0001} crystal planes of wurtzite ZnO, which further proves that ZnO rod arrays prepared in the present system grew along their *c*-axes.

Figure 5 shows the typical XRD patterns of representative ZnO architectures on different substrates including glass, Pt/

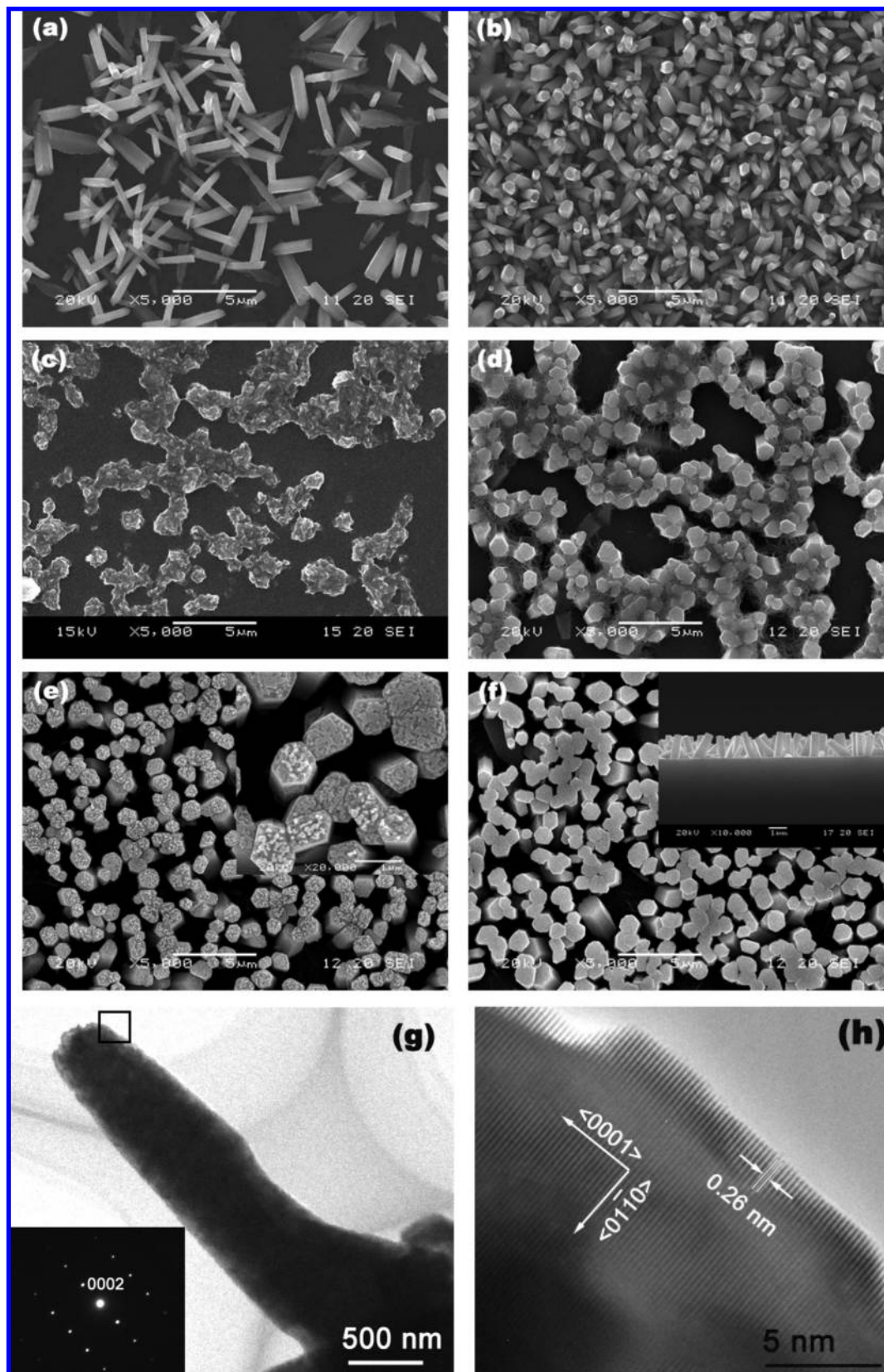


Figure 4. Plan view and cross-sectional SEIs of ZnO architectures grown on glass substrates under different growth conditions: (a) 0.005 M, 70 °C, 1 h; (b) 0.005 M, 70 °C, 3 h; (c) 0.05 M, 90 °C, 1 h; (d) 0.05 M, 90 °C, 3 h; (e) 0.05 M, 90 °C, 6 h; (f) 0.05 M, 90 °C, 10 h. (g) Low-resolution TEM image of an individual ZnO rod peeled from the ITO glass substrate and its corresponding SAED pattern (inserted at the up-left corner). (h) HRTEM image taken from the area marked with the black frame in (g).

glass, Au/glass, and ITO/glass. All diffraction peaks can be indexed to wurtzite (hexagonal) structured ZnO (space group $P6_3mc$) with cell parameters $a = 3.249 \text{ \AA}$ and $c = 5.206 \text{ \AA}$,

which is in good agreement with the literature values (JCPDS card, No. 36-1451). No characteristic peaks of other impurities were detected in the patterns, suggesting that only single-phase

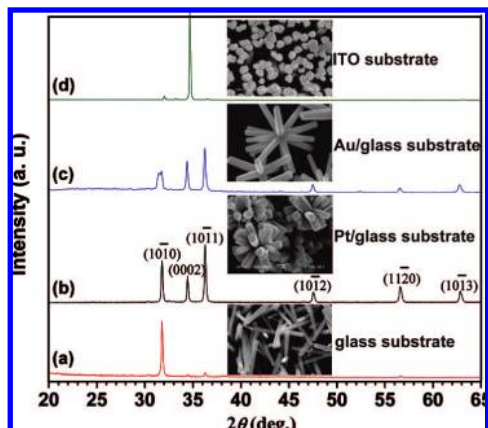


Figure 5. XRD patterns of the representative ZnO architectures as thin film on different substrates: (a) glass substrate; (b) Pt/glass substrate; (c) Au/glass substrate; (d) ITO/glass substrate.

ZnO samples were formed. The sharp diffraction peaks indicate the good crystallinity of the synthesized ZnO products. From these XRD data, we can illustrate the texture effect of the anisotropic morphology and orientation on the relative intensity of the diffraction peak (normalized to the $\langle 10\bar{1}1 \rangle$ peak, which usually corresponds to the maximum intensity of the ZnO diffraction peak). It is notable that, except the ZnO sample with flowerlike morphology on the Pt/glass substrate (Figure 5b), the relative intensities of XRD diffraction peaks of ZnO samples on other substrates differ from the standard pattern of the bulk materials, which should be caused by preferred orientation and different assembly pattern of the ZnO crystals with various shapes on the substrate surface.³⁶ As expected, a substantially higher intensity is observed for the $\langle 0002 \rangle$ diffraction peak in the XRD patterns of ZRAs on the ITO/glass substrate (Figure 5d), indicating that the ZRAs are highly oriented with their c -axes being perpendicular to the substrate, which is well consistent with the SEI results in Figure 4. For the XRD pattern of ZnO sample (rodlike crystals) on the glass substrate (Figure 5a), only a high intensity $\langle 10\bar{1}0 \rangle$ peak is observed and other diffraction peaks are un conspicuous, which indicates most of the rodlike ZnO crystals on the glass slice were orientated with their c -axes parallel to the substrate during the growth period, as shown in Figure 1. As for the ZnO sample composed of stelliform crystals on Au/glass, its XRD pattern exhibits that $\langle 0002 \rangle$ diffraction intensity is higher than parallel of $\langle 10\bar{1}0 \rangle$ (see Figure 5c). This observation corresponds to the fact that ZnO architectures of stelliform crystals consist of rodlike crystals partly vertical to the substrate, as displayed in the SEIs of Figure 3c and d. Chemical composition of the as-prepared samples was obtained using an EDS. Figure 6 shows the EDS result of the as-grown ZnO films composed of rod arrays on the ITO/glass substrate. The EDS pattern indicates that only two essential constituents such as Zn and O were detected from the obtained spectrum. Quantitative analysis shows that the mean atomic ratio of Zn/O of ZnO rod is 0.494:0.506. No evidence of other impurities was detected, and the ZnO rod is nearly stoichiometric. These data also confirm the high purity of the as-synthesized ZnO samples. All the ZnO samples on other substrates also exhibit the similar EDS results (not shown).

The room-temperature PL spectra of typical ZnO architectures on different substrates including glass, Pt/glass, Au/glass, and ITO/glass were obtained with an excitation wavelength of 325 nm and are shown in Figure 7. In order to eliminate the interference from the substrate, those samples with maximal coverage were selectively used. A strong and sharp ultraviolet

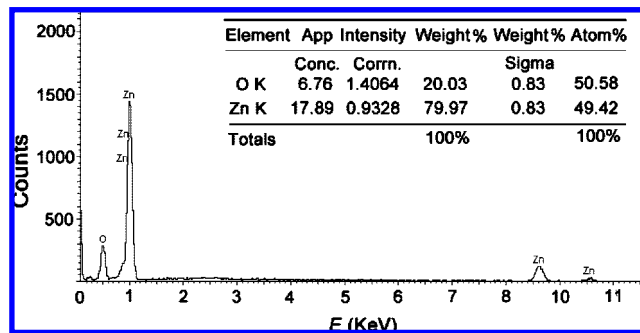


Figure 6. EDS result of the as-synthesized ZnO film composed of rod arrays on the ITO/glass substrate.

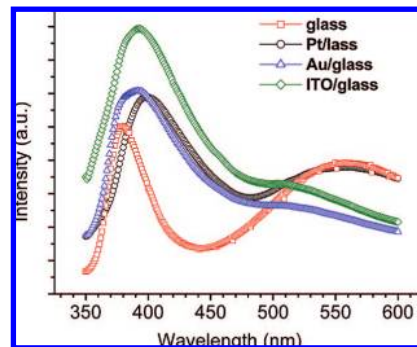


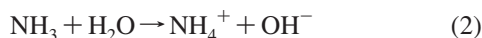
Figure 7. Room-temperature photoluminescence spectra of ZnO architectures as thin film on different substrates, including glass substrate, Pt/glass substrate, Au/glass substrate, and ITO/glass substrate with an excitation wavelength of 325 nm.

(UV) emission band dominates all the PL spectra. The UV emission also called the near band edge emission (NBE) may originate from free excitonic emission in the ZnO materials^{15,37,38} as ZnO has a high exciton-binding energy of 60 meV at room temperature.² It is observed that there is a shift in position in peaks, which could be due to different native defect and free carrier concentrations in different samples. ZnO rodlike crystals on the glass substrate show a UV emission peak (full width-half-maximum (fwhm) = 28 nm) at 380 nm (3.26 eV). The ZnO sample with flowerlike morphology on the Pt/glass substrate also shows a UV emission peak (fwhm = 50 nm) at 399 nm (3.12 eV). A similar UV emission peak (fwhm = 55 nm) at 392 nm (3.15 eV) is observed for ZnO architectures on both Au/glass and ITO/glass substrates, the only difference being the relative intensity of peaks.

Besides the strong UV emission peak, there is a broad green emission band starting from 500 nm that lies in the visible region. The visible emission generally nominated as deep level emission (DLE) is probably related to the variation of the intrinsic defects in ZnO films, such as zinc vacancy (V_{Zn}), oxygen vacancy (V_O), interstitial zinc (Zn_i), interstitial oxygen (O_i), and antisite oxygen (O_{Zn}).^{39–43} In a word, the origin of the visible emission in ZnO is highly controversial. Visible emissions are commonly observed in the solution chemical synthesized ZnO nanostructures. The green PL has been found in ZnO crystals grown by hydrothermal,⁴⁴ vapor–liquid–solid epitaxial (VLSE),^{45,46} chemical vapor deposition (CVD),⁴⁷ and electrochemical methods,⁴⁸ and its origin is widely ascribed to the recombination of the photogenerated holes with the single ionized V_O .^{49,50} More singly ionized oxygen V_O defects will result in a higher green PL intensity. However, the PL spectra in Figure 7 illustrate that this broad green peak is un conspicuous for the samples on both Au/glass and ITO/glass substrates. In view of

the above analysis, generally speaking, comparing the ratio of the relative PL intensity of the excitonic emission to the DLE ($I_{\text{exc}}/I_{\text{DLE}}$) is a way to evaluate the crystal quality of the ZnO films.³¹ Therefore, in our PL results, the high intensity ratio of $I_{\text{exc}}/I_{\text{DLE}}$ in Figure 7 is an evidence of high crystal quality of ZnO architectures deposited from the $\text{Zn}(\text{NO}_3)_2$ and HMT solution due to weak visible emissions from low intrinsic defects, except the sample deposited on the unmodified glass substrate.

To understand the observed different assembly patterns of ZnO architectures, it is necessary to study their growth mechanism on different substrates. As a wurtzite-structured metal oxide, ZnO belongs to the $P6_3mc$ space group and has a highly anisotropic structure along the c -axis. The (0001) plane (terminated with zinc) of ZnO has the maximum surface energy, while the (000 $\bar{1}$) plane (terminated with oxygen) has the minimum surface energy. As a result, the growth along the [0001] direction has a faster rate than along other directions and is much more favorable. Therefore, 1D wirelike or rodlike structures of ZnO are readily formed. The growth of ZnO crystals is also controlled by nucleation and growth processes in aqueous solution. In the present reaction system, the possible formation process of hexagonal ZnO phase by ACG can be expressed as follows:



On the basis of surface energy minimization, ZnO crystallites from zinc hydroxyl nucleate along the c -axis and then grow into 1D rodlike crystals (Figure 1a and b). When the precursor concentration increases, the nucleation of ZnO is so rapid that more ZnO nuclei form in the initial stage. These nuclei may aggregate together due to supersaturation. Each of them individually grows along the c -axis into a rodlike crystal, and thus, flowerlike or stelliform architectures are finally formed (Figure 2c and d and Figure 3c and d). It was interestingly found from Figure 1c–f that increasing growth duration resulted in dissolution of rodlike crystals to some extent and yielded double-tip rodlike and needlelike crystals. This phenomenon can be related to the growth mechanism of a single crystal: growth-dissolution-recrystallization,⁵² which corresponds to eq 4 and the reversible reaction (eq 5) for a longer growth duration. In the previous reports,³³ this mechanism has been verified by investigating the effect of growth time and solution temperature on the morphology of ZnO structures.

A suitable substrate may be helpful for nucleation and subsequent flowerlike or stelliform growth of ZnO architectures. Comparing Figure 1c and d with Figure 2c and d and Figure 3c and d, one can observe that the substrates play a critical role in determining the assembly of ZnO architectures under the same growth conditions. ZnO architectures on Pt/glass or Au/glass substrates exhibit 3D assembly patterns of ZnO crystals and seem to be first adsorbed on Pt or Au crystallites sputtered on glass substrates and then nucleate. However, ZnO samples on glass substrates without Au- or Pt-sputtering were composed of many individual rodlike crystals and scattered randomly on the substrate. In addition, compared with Figure 2a and b and Figure 3a and b, Figure 2c and d and Figure 3c and d exhibit higher coverage of the substrate area and more integrated

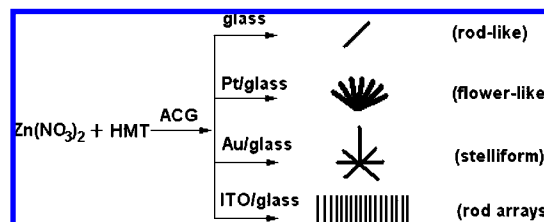


Figure 8. Schematic illustration of ZnO architectures on various substrates.

architecture. Nucleation is the first process required for crystallization in a supersaturation solution and can be tuned by controlling experimentally its interfacial tension. Any adsorption phenomenon at the interface decreases the interfacial tension. Such effect is described quantitatively by Gibbs adsorption equation: $d\gamma = -\sum_i \Gamma_i d\mu_i$,³⁰ where γ represents the interfacial tension, Γ represents the superficial adsorption density, and μ represents the chemical potential of adsorbed species i . Therefore, on Pt/glass or Au/glass substrates, the interfacial tension of the system will reach a minimum. Meanwhile, a maximum is found for the first derivative of the free enthalpy of nucleation. Such a maximum depends on the interfacial tension at the cubic power: $\Delta G^* = 16\pi\nu^{-2}\gamma^3/3(RT\ln S)^2$.³⁰ Thus, reducing the interfacial tension leads to an important decrease of the nucleation energy barrier. On the other hand, supersaturation is required for crystal growth. Comparatively high supersaturation will lower the activation energy needed by crystal growth, resulting in an increase of the crystal growth rate. As for the ITO substrates, ZnO architectures consisted of vertically aligned ZnO rod arrays directly grown on the substrate, which shows that the ITO substrate has low interfacial tension and ZnO tiny crystallites can directly adsorb on the substrate and then nucleate. The possible growth routes of these as-synthesized ZnO architectures on different substrates by ACG can be schematically illustrated in Figure 8.

On the basis of the above preliminary experiments and analysis, four types of assembly patterns of ZnO architectures were achieved by both inherent structural characteristics of ZnO and external experimental conditions (i.e., various substrates in our case). Other external factors, such as growth duration, solution temperature, and precursor concentration mainly influenced the size and morphology of ZnO crystals. More in-depth studies are necessary to further understand their growth process, which can provide important information for crystal design and assembly controlled synthesis of ZnO architectures and other metal oxide systems.

4. Conclusions

In summary, we successfully realized preliminary control over assembly patterns of ZnO architectures (rodlike, flowerlike, urchinlike, stelliform, and rod arrays) by varying different substrates including glass, Pt/glass, Au/glass, and ITO/glass through a facile ACG method. These substrates were sensitive to solution conditions and were contrived to provide a carrier for nucleation and growth. The possible growth mechanisms for different assembly patterns dependent on the substrate were proposed. It was revealed that both the inherent highly anisotropic structure of ZnO and surface energy minimization of different substrates play crucial roles in determining final morphologies of ZnO architectures. Moreover, the room-temperature photoluminescence (PL) properties of ZnO architectures on various substrates were investigated, and the strong UV emission but weak defect-related DLE indicated that the

as-synthesized samples are of good crystal quality, except the sample deposited on the unmodified glass substrate.

References and Notes

- (1) Tüzemen, S.; Gür, E. *Opt. Mater.* **2007**, *30*, 292.
- (2) Roy, V. A. L.; Djurisic, A. B.; Chan, W. K.; Cao, J.; Lui, H. F.; Surya, C. *Appl. Phys. Lett.* **2003**, *83*, 141.
- (3) Hirai, T.; Harada, Y.; Hashimoto, S.; Itoh, T.; Ohno, N. *J. Lumin.* **2005**, *112*, 196.
- (4) Tadashi, S.; Akira, K. *Appl. Phys. Lett.* **1974**, *25*, 10.
- (5) Jia, C. L.; Wang, K. M.; Wang, X. L.; Zhang, X. J.; Lu, F. *Opt. Express* **2005**, *13*, 5093.
- (6) Sharma, P.; Sreenivas, K. *Appl. Phys. Lett.* **2003**, *83*, 3617.
- (7) Hsueh, T. J.; Chen, Y. W.; Chang, S. J.; Wang, S. F.; Hsu, C. L.; Lin, Y. R.; Lin, T. S.; Chen, I. C. *Sens. Actuat. B-Chem.* **2007**, *125*, 498.
- (8) Park, S. H.; Kim, S. H.; Han, S. W. *Nanotechnology* **2007**, *18*, 055608.
- (9) Basudev, P.; Batabyal, K. B.; Amlan, J. P. *Sol. Energy Mater. Sol. Cells* **2007**, *91*, 769.
- (10) Chan, E. M.; Mathies, R. A.; Alivisatos, A. P. *Nano Lett.* **2003**, *3*, 199.
- (11) Milliron, D. J.; Hughes, S. M.; Cui, Y.; Manna, L.; Li, J.; Wang, L. W.; Alivisatos, A. P. *Nature* **2004**, *430*, 190.
- (12) Vayssieres, L. *Adv. Mater.* **2003**, *15*, 464.
- (13) Wang, Z. L.; Song, J. H. *Science* **2006**, *312*, 242.
- (14) Qin, Y.; Wang, X. D.; Wang, Z. L. *Nature* **2008**, *451*, 809.
- (15) Huang, L. S.; Wright, S.; Yang, S. G.; Shen, D. Z.; Gu, B. X.; Du, Y. W. *J. Phys. Chem. B* **2004**, *108*, 19901.
- (16) Huang, L. S.; Pu, L.; Shi, Y.; Zhang, R.; Gu, B. X.; Du, Y. W.; Zheng, Y. D. *Opt. Express* **2005**, *13*, 5263.
- (17) She, G. W.; Zhang, X. H.; Shi, W. S.; Fan, X.; Chang, J. C. *Electrochem. Commun.* **2007**, *9*, 2784.
- (18) Hu, J. Q.; Li, Q.; Meng, X. M.; Lee, C. S.; Lee, S. T. *Chem. Mater.* **2003**, *15*, 305.
- (19) Gao, P. X.; Ding, Y.; Mai, W. J.; Hughes, W. L.; Lao, C. S.; Wang, Z. L. *Science* **2005**, *309*, 1700.
- (20) Lao, J. Y.; Wen, J. G.; Ren, Z. F. *Nano Lett.* **2002**, *2*, 1287.
- (21) Shen, G. Z.; Bando, Y. S.; Lee, C. J. *J. Phys. Chem. B* **2005**, *109*, 10578.
- (22) Xu, C. X.; Sun, X. W.; Chen, B. J.; Dong, Z. L.; Yu, M. B.; Zhang, X. H.; Cua, S. J. *Nanotechnology* **2005**, *16*, 70.
- (23) Shen, G.; Cho, J. H.; Lee, C. J. *Chem. Phys. Lett.* **2005**, *401*, 414.
- (24) Khan, A.; Kordesch, M. *Physica E* **2005**, *30*, 51.
- (25) Zhang, J.; Yang, Y.; Xu, B.; Jiang, F.; Li, J. *J. Cryst. Growth* **2005**, *280*, 509.
- (26) Ye, C. H.; Fang, X. S.; Hao, Y. F.; Teng, X. M.; Zhang, L. D. *J. Phys. Chem. B* **2005**, *109*, 19758.
- (27) Muthukumar, S.; Gorla, C. R.; Emanetoglu, N. W.; Liang, S.; Lu, Y. *J. Cryst. Growth* **2001**, *225*, 197.
- (28) Zhang, Z. Z.; Shen, D. Z.; Lu, Y. M.; Zhang, J. Y.; Li, B. H.; Zhao, D. X.; Yao, B.; Fan, X. W. *J. Lumin.* **2007**, *122–123*, 202.
- (29) Ayadi, Z. B.; Mir, L. E.; Djessas, K.; Alaya, S. *Mater. Sci. Eng., C* **2008**, *28*, 613.
- (30) Vayssieres, L. *Int. J. Nanotechnol.* **2004**, *1*, 1.
- (31) Ndifor-Angwafor, N. G.; Riley, D. J. *Phys. Stat. Sol. (a)* **2008**, *205*, 2351.
- (32) Vernardou, D.; Kenanakis, G.; Vlachou, K.; Koudoumas, E.; Kiriakidis, G.; Vairis, A.; Katsarakis, N. *Phys. Stat. Sol. (c)* **2008**, *5*, 3348.
- (33) Vernardou, D.; Kenanakis, G.; Couris, S.; Manikas, A. C.; Voyiatzis, G. A.; Pemble, M. E.; Koudoumas, E.; Katsarakis, N. *J. Cryst. Growth* **2007**, *308*, 105.
- (34) Masuda, Y.; Kinoshita, N.; Sato, F.; Koumoto, K. *Cryst. Growth Des.* **2006**, *6*, 75.
- (35) Umar, A.; Kim, S. H.; Kim, J. H.; Park, Y. K.; Hahn, Y. B. *Mater. Lett.* **2007**, *61*, 4954.
- (36) Andelman, T.; Gong, Y.; Polking, M.; Yin, M.; Kuskovsky, I.; Neumark, G.; O'Brien, S. *J. Phys. Chem. B* **2005**, *109*, 14314.
- (37) Chen, Y.; Bagnall, D. M.; Koh, H. J.; Park, K. T.; Hiraga, K.; Zhu, Z.; Yao, T. *J. Appl. Phys.* **1998**, *84*, 3912.
- (38) Greene, L. E.; Law, M.; Goldberger, J.; Kim, F.; Johnson, J. C.; Zhang, Y. F.; Saykally, R. J.; Yang, P. D. *Angew. Chem., Int. Ed.* **2003**, *42*, 3031.
- (39) Gao, Y. F.; Nagai, M.; Masuda, Y.; Sato, F.; Koumoto, K. *J. Cryst. Growth* **2006**, *286*, 445.
- (40) Liu, B.; Fu, Z.; Jia, Y. *Appl. Phys. Lett.* **2001**, *79*, 943.
- (41) Vanheusden, K.; Seager, C. H.; Warren, W. L.; Tallant, D. R.; Voigt, J. A. *Appl. Phys. Lett.* **1996**, *68*, 403.
- (42) Khan, A.; Kordesch, M. *Mater. Lett.* **2008**, *62*, 230.
- (43) Khan, A.; Jadwisieniczak, W. M.; Kordesch, M. *Physica E* **2006**, *33*, 331.
- (44) Zhang, J.; Sun, L. D.; Pan, H. Y.; Su, H. L.; Liao, C. S.; Yan, C. H. *Chem. Mater.* **2002**, *14*, 4172.
- (45) Huang, M. H.; Wu, Y.; Feick, H.; Tran, N.; Weber, E.; Yang, P. *Adv. Mater.* **2001**, *13*, 113.
- (46) Wang, X.; Song, J.; Li, P.; Ryou, J. H.; Dupuis, R. D.; Summers, C. J.; Wang, Z. L. *J. Am. Chem. Soc.* **2005**, *127*, 7920.
- (47) Wu, J. J.; Liu, S. C. *Adv. Mater.* **2002**, *14*, 215.
- (48) Xu, F.; Lu, Y. N.; Xie, Y.; Liu, Y. F. *Vacuum* **2009**, *83*, 360.
- (49) Guo, M.; Diao, P.; Cai, S. M. *J. Solid State Chem.* **2005**, *178*, 1864.
- (50) Wu, X. L.; Siu, G. G.; Fu, C. L.; Ong, H. C. *Appl. Phys. Lett.* **2001**, *78*, 2285.
- (51) Gu, C. D.; Li, J.; Lian, J. S.; Zheng, G. Q. *Appl. Surf. Sci.* **2007**, *253*, 7011.
- (52) Govender, K.; Boyle, D. S.; Kenway, P. B.; O'Brien, P. *J. Mater. Chem.* **2004**, *14*, 2575.

JP808456R